Physics of High Power Impulse Magnetron Sputtering

André Anders[1*], Joakim Andersson[1], David Horwat[1], and Arutiun Ehiasarian[2]

[1]Lawrence Berkeley National Laboratory, University of California, 1 Cyclotron Road, Berkeley, California 94720, USA
[2]Materials and Engineering Research Institute, Sheffield Hallam University, Howard St., Sheffield S1 1WB, UK
*Presenting and corresponding author; aanders@lbl.gov

Abstract

High power impulse magnetron sputtering is characterized by discharge pulses whose target power density exceeds conventional sputtering power densities by two orders of magnitude or more; the goal is to provide a large flux of ionized sputtered material. The processes of pulse evolution are briefly reviewed, including secondary electron emission, self-sputtering, and rarefaction. Using a pulse power supply capable of providing constant voltage for target peak power densities up to 5 kW/cm^2, the evolution of the current-voltage characteristics was investigated for copper and titanium. It is shown that the characteristic cannot be reduced to value pairs. Rather, a strong but reproducible development exists. The details depend on the argon pressure and applied voltage. Each target material exhibits a distinct and sharp transition to a high current regime that appears to be dominated by metal plasma. Despite the higher sputter yields for copper, the transition to the high current regime occurs much earlier and stronger for titanium, which may be attributed to a higher secondary electron yield and hence a higher density of electrons confined in the magnetron structure. At high currents, the closed-drift Hall current generates a magnetic field that weakens plasma confinement, thereby enabling large ion currents to reach a biased substrate.

1. Introduction

High Power Impulse Magnetron Sputtering (HIPIMS) is a young physical vapor deposition (PVD) technology. Researchers make rapid progress in exploring its potential and limitations. It is characterized by very high pulse power density, which is typically two orders of magnitude greater than the average power density. We chose the term HIPIMS, as opposed to high power pulse sputtering (HPPMS), which is inconsistently used for either HIPIMS-like systems or for medium frequency pulsed sputtering with large area targets. In the latter case, even as the power is high, the pulse power *density* does not much exceed the average power density. With greatly enhanced power density, new physical processes are enabled, in particular the ionization of sputtered atoms. The presence of ionized sputtered material is of great importance to some PVD applications such as filling of trenches and vias of semiconductor microprocessors. Additionally, HIPIMS may be used for applications that are traditionally served by cathodic arc plasma processing such as substrate etching [1] film deposition [2].

The roots of ionized sputtering may be traced back to research in Japan some 30 years ago when Hosokawa and coworkers noticed a discrepancy between the measured and calculated copper and aluminum deposition rates [3]. They estimated that, in the case of aluminum, about 18% of the ion current could be due to ionized sputtered atoms, which can cause self-sputtering. A few years later, they published a condition for sustained self-sputtering, i.e., a condition for sputtering that exclusively relies on self-sputtering. Argon, or a similar gas, is only needed to get the process started and may well be shut off afterwards [4]. The sustained sputter process can operate with ionized metal only provided the power density is very high (typically several 100 W/cm^2 [5]). The condition reads

$$\alpha\beta\gamma_{SS} \geq 1 \qquad (1)$$

where α is the ionization probability, β is the probability that a sputtered and ionized atom will return to the target, and γ_{SS} is the self-sputter yield. Since $\alpha \leq 1$ and $\beta < 1$, the condition $\gamma_{SS} > 1$ is necessary but not sufficient for sustained self-sputtering.

Sustained self-sputtering has been demonstrated for a very limited number of materials by several researchers. For example, Posadowski and Radsimski [6] showed that the principle works for copper and silver, which are metals of very high self-sputter yield. The experiments showed that sustaining the self-sputtering without processing gas required operation with a high current density on the target. This suggested to go to even higher current density (or, equivalently, power density), which is only possible by using pulses, in order to not exceed the average power rating of the magnetron.

At a 1996 symposium in Berkeley, Sergey Bugaev and coworkers [7] reported about pulsing a filament-assisted, hollow cathode magnetron to high power, with pulse voltage up to 800 V and peak current of 450 A, leading to a deposition rate of copper of 11 μm/min.

In 1999, Kouznetsov and coworkers [8] published their much-cited work in which they explicitly outline the possibility to operate a magnetron at very high power density, with peak power soon to approach the 1 MW level, leading to deposition of the target material from the plasma phase, as opposed to "vapor" of neutral atoms. The number of papers in the field of HIPIMS has grown since. Yet, many aspects of the complicated physics have not been fully understood. In the following, we will present first a very brief summary on the physics of HIPIMS. Then we will report on original experiments shedding light on some of the discharge physics.

2. Some basic physics of the HIPIMS

In the following discussion we initially neglect the important contribution of the magnetic field. We do this for the sake of simplicity with the argument that this field is not strong enough to magnetize ions but only electrons. This could be justified as long as the electron density in the sheath is much smaller than the ion density and the ion motion within the sheath is only marginally affected by the magnetic field—conditions to be further explored. Of course, the magnetic field plays an important role, especially for the closed-drift motion of electrons, the probability of generating ions by impact ionization, and the ambipolar diffusion towards the substrate.

As the voltage pulse is applied to the target (the cathode of the magnetron discharge), the sheath expands initially with the characteristic time of the inverse electron plasma frequency. This is generally in the sub-microsecond regime, and hence the electron response is typically determined by the pulse rise time rather than electron inertia. The sheath expands as the (argon) ions are accelerated towards the target surface; the thickness asymptotically approaches the new equilibrium value. If we take the Child law, which can be applied to determine the thickness of a collisionless sheath [9], we have

$$s = \frac{3}{4}\left(\frac{\varepsilon_0^2 V_{sheath}^3}{e\, n_0^2 kT_e}\right)^{1/4}, \qquad (2)$$

where ε_0 is the permittivity of free space, e is the elementary charge, k is the Boltzmann constant, V_{sheath} is the voltage drop in the sheath, n_0 is the plasma density, and T_e is the temperature of plasma electrons; Fig. 1 shows the width for relevant voltage and plasma parameters.

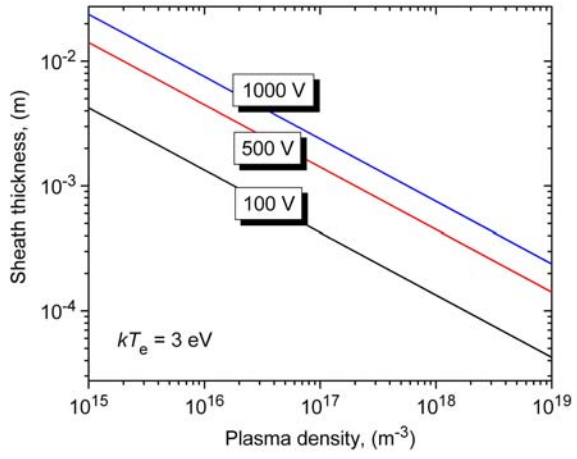

Fig. 1 Child sheath thickness as a function of plasma density, with electron temperature and sheath voltage as parameters.

The physics of the plasma immersion ion implantation (PIII) can be applied, see the extensive discussion by Wood and coworkers [10], following original contributions by Lieberman and others [11, 12].

The sheath evolution is greatly affected by the pre-pulse plasma density near the target: in the case of widely spaced pulses, and absence of a "keeping" plasma, the rise of current is often substantially delayed with respect to the applied voltage due to a statistical time lag for electrons to develop an avalanche and finally plasma. The example shown in the original Kouznetsov paper [8] is typical for this situation. A low-power "keeping" discharge or operation at high duty cycles ensures that the applied HIPIMS pulse can immediately lead to a strong rise in discharge current because there are enough ions near the target available to be accelerated. In contrast to conventional PIII models, the plasma density is strongly dependent on the fluxes of secondary electrons and sputtered atoms coming from the target. The new sheath thickness is a complicated issue because the plasma evolves, too, and not just the sheath.

Ions impacting the target surface cause two main secondary processes: (i) emission of secondary electrons and (ii) sputtering of atoms. Both processes are critical and deserve deeper considerations.

Secondary electrons (SE) are crucial for maintaining the discharge because they gain energy by traveling through the electric field of the sheath; they can directly cause ionization by impact ionization or indirectly via heating of the less energetic electrons in the bulk of the energy distribution function (plasma electrons).

The trajectory of a secondary electron is immediately curved due to the magnetic field of the magnetron when it is leaving the target surface. The electron gyration radius is

$$r = \frac{m_e v_\perp}{eB} = \sqrt{\frac{2V_e m_e}{eB^2}} \qquad (3)$$

where m_e is the electron mass, $v_\perp$ is the velocity vector perpendicular to the direction of the magnetic field, V_e is the corresponding energy (in volt), and B is the magnetic induction.

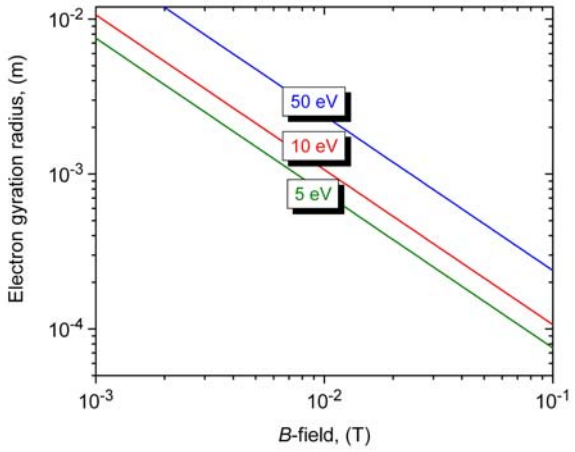

Fig. 2 Electron gyration radius as a function of magnetic field and energy perpendicular to the field lines.

Whereas electrons from the plasma cannot penetrate the sheath due to the repelling field, secondary electrons are unable to readily leave the sheath due to trapping by the magnetic field: Fig. 2 shows that the electron gyration radius is comparable to or smaller than the Child sheath (Fig. 1). This has

interesting implications, namely, that (i) the Child sheath is at best good for an estimate, (ii) the positive space charge in the sheath is "diluted" by magnetically trapped electrons, and therefore the actual sheath thickness will be larger than the Child sheath, (iii) secondary electrons are trapped and can cause ionization within the sheath, (iv) collisions must happen in the sheath, enabling secondary electrons to leave the sheath; collisions are the rule, not just a side effect.

If an ion is formed within the sheath, it will be accelerated toward the target surface and will cause further secondary electron emission (SEE) and sputtering. The yield of SEE facilitated by kinetic energy ("kinetic emission") is less than 0.1 for the energy range of interest (~ 1 keV or less), whereas "potential emission" depends on the potential energy of the arriving ion and the work function of the emitting material. Potential emission requires that the ionization energy of the arriving ions exceeds twice the workfunction of the material ϕ; experimental data of the yields for various ions satisfy the fit [13]

$$\gamma_{PSE} = 0.032\left(0.78E_i - 2\phi\right). \qquad (4)$$

A secondary electron will be accelerated after leaving the solid by the electric field of the sheath. The electron picks up significant energy in the fist half cycle of its gyration motion; the exact amount depends on the potential difference between target surface and the most distant point from surface. It periodically gains and loses energy as the gyration occurs, and additionally it drifts perpendicularly to both the electric and magnetic field vectors ($\mathbf{E}\times\mathbf{B}$ drift). During its motion, the electron can generate many ion-electron pairs through ionizing collisions.

Much has been written about sputtering [14-16] and ionized sputtering [1, 17, 18]. For the latter, a key issue is to use process parameters and a suitable geometry such that the probability of ionization is high for the sputtered atoms before they reach the substrate. This is generally achieved by increasing the background gas pressure, making it likely that the sputtered atoms collide thereby slowing them down for a longer residence time in the plasma.

Considering a one-dimensional model description and using z as the coordinate normal to the target surface, the flux of sputtered atoms from the surface is reduced by [19]

$$d\Gamma_a = -\sigma_{ag}\,\Gamma_a\,n_g\,dz \qquad (5)$$

where σ_{ag} is the cross section for atom-gas collision, and n_g is the gas density, with

$$n_g = p/kT_g\,, \qquad (6)$$

p is the pressure, and T_g the gas temperature. If σ_{ag} is independent of position, one obtains

$$\Gamma_a(z) = \Gamma_a(0)\exp\left(-z/\lambda_{ag}\right) \qquad (7)$$

with the mean free path

$$\lambda_{ag} = \frac{1}{n_g\sigma_{ag}} = \frac{kT_g}{p\sigma_{ag}}\,, \qquad (8)$$

where we used the ideal gas equation. The cross section σ_{ag} is not precisely known for all the atom-gas combinations, but it is generally $(10-40)\times10^{-20}\,\mathrm{m}^2$, with the lower values at higher kinetic energy of the colliding particles. Note that the Eq. (8) includes the rarefaction effect, namely, as the local temperature increases during operation, the local gas density decreases and the mean free path increases proportionally. Fig. 3 shows the mean free path assuming the gas at room temperature.

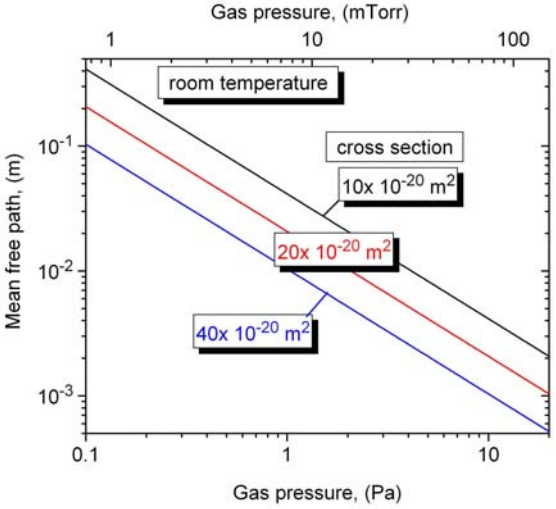

Fig. 3 Parametric presentation of the mean free path for fast atoms in gas; the mean free path increases proportionally with the gas temperature.

At a typical pressure of, say, 1 Pa (7.5 mTorr), the mean free path is larger than the sheath thickness, and only a fraction $f \approx s/\lambda_{ag}$ of sputtered atoms will be slowed by a collision. The important effect of collisions, apart from increasing the chance of ionization, is the feedback that slowed sputtered atoms can provide: they themselves can become part of the "gas" that can slow down sputtered atoms. That means the gas density n_g in Eq.(5) is a highly dynamic variable, depending both on heating (rarefaction) and generation of slowed sputtered atoms. Clearly, these processes evolve during the pulse duration, and therefore the following section focuses on experiments with rather long pulse length, which should help to understand the role of metal "vapor" for the operation of a HIPIMS discharge.

3. HIPIMS experimental setup

In our experiments, we studied the current voltage characteristic of HIPIMS discharges for different target materials and different process gas pressures using—for clarity—a discharge system in constant voltage mode. To keep it simple, we focused on the metallic mode, using pure argon gas only.

A 2-inch (5 cm) planar, balanced magnetron was used. The targets were ¼ inch (6.25 mm) thick; the magnetic field induction at the center of the target surface was 64 mT. We intentionally used such a small magnetron because it allowed us to access the region of very high power density (peak up to 5 kW/cm^2 averaged over the target area). The power was supplied

by a slightly modified SPIK2000A pulse power supply (Melec GmbH) operating in the unipolar negative mode. A great feature of this pulser is the ability to freely adjust the individual pulse length. The short pulse limit is given by the circuit to 5 μs, and the long limit by the stored energy, which practically means milliseconds. We are especially interested in long pulses. However, the allowable average power to the magnetron (1 kW) was a limiting factor that needed to be taken into account. Hence, long pulse operation necessarily implied long pauses between pulses. The nominal voltage of the pulser was adjustable up to 1000 V. The arc threshold was set to 150 A, at which the arc suppression mechanism would be triggered, rapidly cutting off the pulse-driving voltage. Unless the applied voltage pulse is cut short by the arc suppression circuit, it is constant for the selected pulse length, i.e. typically 400 μs. In the case of Ti and high voltage, we had to use shorter pulses to protect the equipment.

Pure argon gas was supplied near the target, establishing an operational pressure that was adjusted by the specific combination of flow rate (up to 100 sccm) and pumping speed (cryo pump and adjustable valve) At fully open valve, the pumping speed was 1500 l/s for air; the chamber base pressure was about 10^{-4} Pa. The total pressure was monitored by an MKS Baratron® gauge.

The discharge current was monitored using a Pearson™ current transformer (model 301X, 0.01 V/A, 2 MHz bandwidth); and the voltage at the target was measured with a Tektronix 1000:1 divider (model 6015A, 75 MHz bandwidth); the data were recorded on a digital storage oscilloscope (Tektronix TDS5104B) in sample mode.

The ion flux was measured using a differentially pumped combined mass and energy analyzer (EQP 300 by HIDEN Ltd.); the entrance aperture was at ground potential with an orifice of 100 μm diameter. The total ion current was recorded using an ion collector of about 100 cm^2 area biased to -50 V with respect to ground. The distance of the analyzer from the target could be adjusted and was typically either 10 or 20 cm.

In this report, we limit data and discussion to copper and titanium – relevant and much-studied materials. Copper is special because its sputter yield is exceptionally high. Titanium has many applications, especially when including its compound films. Fig. 4 shows sputter yields for argon ion and self-ion impact calculated by the SRIM2006 Monte Carlo Code [20].

4. Results for copper

The results for copper at different target voltage are compiled in Fig. 5.

As the pulsed voltage approaches 500 V, one can clearly see the development of an initial current peak of several amperes. Many HIPIMS systems use relatively short pulses of typically 10-50 μs, and this pulse is seen as *the* main feature. With long pulses, however, one needs to acknowledge that the current is greatly reduced at later times, which can be ascribed to rarefaction due to heating.

If we assume that the sheath edge has reached its quasi-equilibrium position, corresponding to the sheath voltage and local plasma density, the current is given by

$$I = (1+\gamma_{SE})\, I_i \qquad (9)$$

where γ_{SE} is the secondary electron yield, averaged over the energy of the impacting ions, and

$$I_i = \int \left(0.61 \overline{Q} e\, n_0\, v_{Bohm}\right) dA, \qquad (10)$$

where $\overline{Q}$ is the average charge state number; the expression in the parenthesis is the Bohm current, with the Bohm velocity

$$v_{Bohm} = \sqrt{kT_e / m_i}\,, \qquad (11)$$

and the integration is over the target area. Rarefaction means that the plasma density at the sheath edge, n_0, is greatly reduced due to heating, which has an immediate effect as seen by Eq.(10).

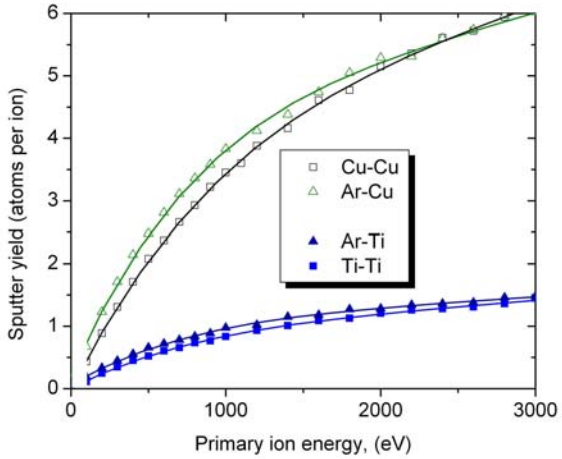

Fig. 4 SRIM-calculated sputtering yields for primary argon ion and self-ion impact. Note that the high primary energies displayed here could be realistically obtained by multiply charged ions at high target voltage.

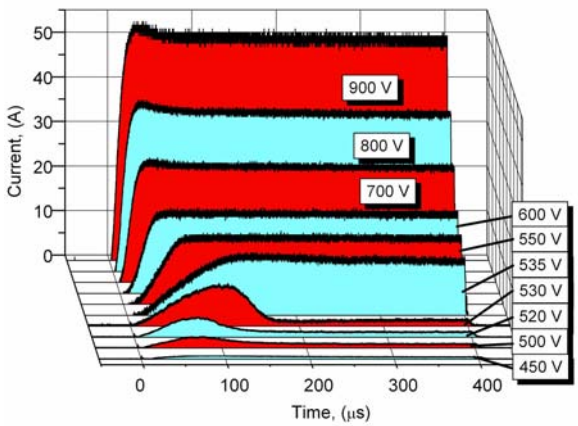

Fig. 5 Current pulse shapes at different constant voltage for copper magnetron discharge (2" target) in argon at 1.8 Pa.

While there are pressure transients in front of the target, the processing chamber acts like a "pressure reservoir," thereby making the heating quasi-isobaric.

The rarefaction behavior changes drastically when the applied "driving" voltage is increased by just

an astonishingly small amount, in the example of Fig. 5 from 530 V to 535 V. The current is not reduced but a new process compensates the current reduction. Given the overwhelming evidence of research on HIPIMS by optical and mass spectroscopy, this can be associated with the appearance of large amounts of copper neutrals and ions, displacing argon. Now the metal starts to greatly affect the discharge.

The ion current collected at 20 cm distance from the target is very small at low driving voltage but shows a remarkable increase after the discharge becomes dominated by metal (Fig. 6); and it becomes disproportionately greater at higher driving voltages.

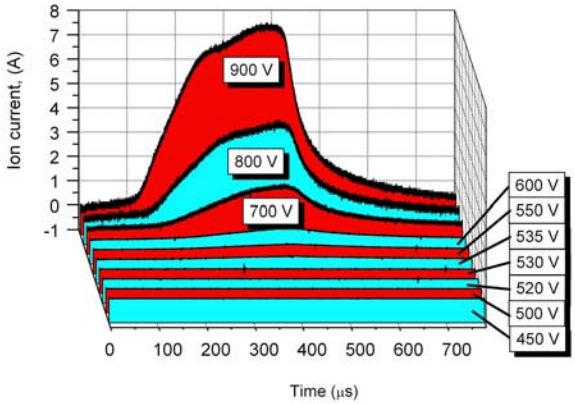

Fig. 6 Ion current of HIPIMS copper discharges as a function of time, with the applied voltage as parameter. These curves correspond to current pulses shown in Fig. 5. The ion collector was 20 cm from the target.

There are several other interesting features in these ion current curves. After about the first 100 μs, the slope of the curves is suddenly steepening, which seems to coincide with the time when metal overtakes rarefaction of argon. This is most pronounced at high voltage (or power). One can also see that the ion current at 20 cm distance tends to increase during the whole pulse even as the discharge parameters appear to have found new steady-state values. This cannot be attributed to the drift processes from the target to the more remote locations of the collector because the delay time between discharge termination and the start of ion current decay is about only 20 μs (i.e., the "information" of pulse termination was transported to the ion collector with about 10^4 m/s). The ion current rise and fall times are much longer, indicative for the importance of metal plasma evolution and collisional processes, including charge exchange.

The disproportional increase of the ion current at high pulse power can be associated with a loss of plasma confinement which is usually provided by the permanent magnetic field. As Rossnagel and Kaufman have shown [21], the circular $\mathbf{E}\times\mathbf{B}$ drift current (Hall current) exceeds the discharge current by about a factor 3.7 (copper target and argon gas). This current is in a doughnut-shape zone just above the "racetrack," where the permanent magnetic field is about 35 mT for our magnetron. A simple estimate of the field generated by the Hall current, I_{ExB}, can be made using the formula

$$B \approx \frac{\mu I_{ExB}}{2\pi r}, \qquad (12)$$

where μ is the permeability of free space, and r is the characteristic distance, such as the height of the "doughnut" above the target (Fig. 7).

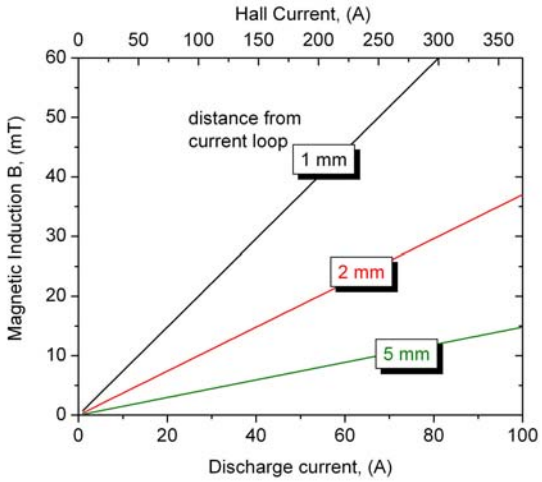

Fig. 7 Magnetic induction, *B*, caused by the closed drift Hall current, which is assumed to be proportional to the discharge current.

As one can see from Fig. 7, when the discharge current reaches the 30-50 A level, the magnetic self-field of the system becomes comparable to the typical 10-30 mT of the permanent magnet in the "racetrack" region, thereby weakening plasma confinement and allowing large amounts of plasma to "leak" from the magnetron.

4. Results for titanium

Based on the sputter yields, Fig. 4, one would expect that less titanium atoms are supplied to the discharge plasma, and that titanium would exhibit the strong metal character at higher powers or later times compared to copper. As shown in Fig. 8, this is not the case.

At low voltage, the current shows a similar behavior as copper, namely a peak at about 50 μs after the initial current rise. It is typical that the initial current rise is delayed by 50 μs or more with respect to the application of the voltage, which defines the time = 0. The current amplitude is higher than copper, which points to the importance of secondary electron emission (SEE).

As mentioned in section 3, potential emission requires that the ionization potential exceeds twice the workfunction of the target material, and therefore singly charged metal ions do not cause potential emission (Table 1).

The ionization energy for doubly charged titanium is lower than the ionization energy for singly charged argon, and therefore one can suspect that a large number of Ti^{2+} is produced, and those ions can produce secondary electrons via potential emission. In contrast, the generation of Cu^{2+} ions requires more energy and therefore less will be present. Less secondary electrons will be emitted, trapped, and

therefore less electrons will contribute to near-target ionization of sputtered material. Additionally, the higher sputter yield of Cu suggests that the electron temperature will be lower than in Ti, further reducing the amount of Cu^{2+} ions produced.

Clearly, there is a need of computer simulation of these processes.

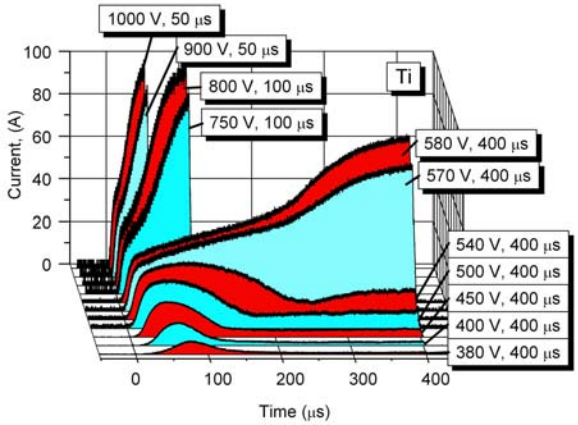

Fig. 8 Current pulse shapes at different constant voltage for Ti discharges in argon at 1.8 Pa. The pulse length for higher driving voltage was precautionary reduced to not damage power supply and magnetron.

	ϕ (eV)	$E_{0\to1}$ (eV)	$E_{1\to2}$ (eV)
Cu	4.9	7.73	20.29
Ti	4.3	6.82	13.58
Ar	n/a	15.76	27.63

TABLE 1. Workfunction, and first and second ionization energies for selected materials.

We conclude by reporting on preliminary measurements using the HIDEN energy and mass analyzer. Fig. 9 shows the flux of different ion species arriving at 10 cm distance, integrated over 50 μs HIPIMS pulses using a Ti target. Despite the relatively short – by the standards of our investigation – pulse length we can clearly see the appearance of titanium ions, including Ti^{2+}. One can also see the rarefaction effect by the fact that the total ion count rate is reduced when the discharge current exceed 10 A.

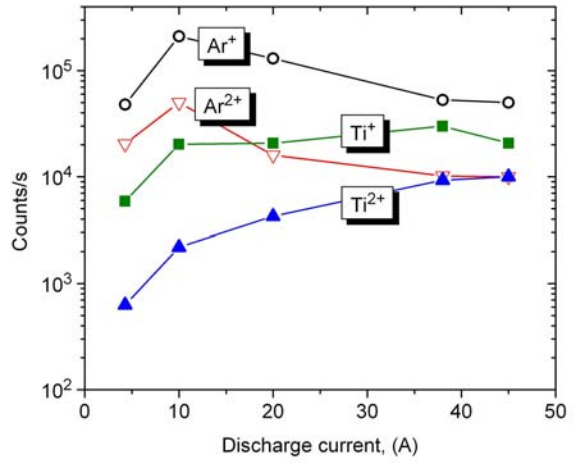

Fig. 9 Ion flux integrated over 50 μs pulses, as a function of peak current, measured 10 cm from the target.

Acknowledgements

We thank G. Mark of Melec GmbH and J. Wallig of Berkeley Lab for technical help. A.E. and J.A. acknowledge support from EPSRC grant EP/D049202/1 and the Wenner-Gren Foundations, respectively. This work was supported by the Assistant Secretary for Energy Efficiency and Renewable Energy, Office of Building Technology, of the U.S. Department of Energy, under Contract No. DE-AC02-05CH11231.

References

[1] A. P. Ehiasarian, J. G. Wen, and I. Petrov, *J. Appl. Phys.* 101 (2007) 054301.
[2] A. P. Ehiasarian, *et al.*, *Surf. Coat. Technol.* 163-164 (2003) 267.
[3] N. Hosokawa, T. Tsukada, and T. Misumi, *J. Vac. Sci. Technol.* 14 (1977) 143.
[4] N. Hosokawa, T. Tsukada, and H. Kitahara, "Effect of discharge current and sustained self-sputtering," Proc. 8th Int. Vacuum Congress, Le Vide, Cannes, France, 1980, 11-14.
[5] W. M. Posadowski, *Thin Solid Films* 392 (2001) 201.
[6] W. M. Posadowski and Z. Radzimski, *J. Vac. Sci. Technol. A* 11 (1993) 2980.
[7] S. P. Bugaev, *et al.*, "Investigation of a high-current pulsed magnetron discharge initiated in the low-pressure diffuse arc plasma," XVIIth Int. Symp. Disch. Electr. Insul. Vacuum, Berkeley, CA, 1996, 1074-1076.
[8] V. Kouznetsov, K. Macak, J. M. Schneider, U. Helmersson, and I. Petrov, *Surf. Coat. Technol.* 122 (1999) 290.
[9] A. T. Forrester, *Large Ion Beams*. New York: Wiley, 1988.
[10] B. P. Wood, *et al.* "Fundamentals of plasma immersion ion implantation," in *Handbook of Plasma Immersion Ion Implantation and Deposition*, A. Anders, Ed. New York: Wiley, 2000, chapter 4.
[11] M. A. Lieberman, *J. Appl. Phys.* 66 (1989) 2926.
[12] R. A. Stewart and M. A. Lieberman, *J. Appl. Phys.* 70 (1991) 3481.
[13] R. A. Baragiola, E. V. Alonso, J. Ferron, and A. Oliva-Florio, *Surface Science* 90 (1979) 240.
[14] M. Kaminsky, *Atomic and Ionic Impact Phenomena on Metal Surfaces*. Berlin: Springer, 1965.
[15] R. Behrisch, (Ed.), *Sputtering by Particle Bombardment I*. Berlin: Springer, 1981.
[16] W. D. Westwood, *Sputter Deposition*. New York: AVS, 2003.
[17] J. A. Hopwood, (Ed.), *Ionized Physical Vapor Deposition*. San Diego, CA: Academic Press, 2000.
[18] U. Helmersson, *et al.*, *Thin Solid Films* 513 (2006) 1.
[19] E. V. Barnat and T.-M. Lu, *Pulsed Sputtering and Pulsed Bias Sputtering*. Boston: Kluwer Academic Publishers, 2003.
[20] J. F. Ziegler and J. Biersack, Monte Carlo code SRIM2006.02, downloadable from http://srim.org/," 2006.
[21] S. M. Rossnagel and H. R. Kaufman, *J. Vac. Sci. Technol. A* 5 (1987) 88.